Xe nuclear magnetic resonance line shapes in channels decorated with paramagnetic centers

Devin N. Sears
Department of Chemistry, University of Alberta, Edmonton Alberta, T6G 2G2, Canada

Lela Vukovic and Cynthia J. Jameson[a)]
Department of Chemistry, University of Illinois at Chicago, Chicago, Illinois, 60607

(Received 30 March 2006; accepted 27 July 2006; published online 20 September 2006)

To make predictions of the Xe NMR line shapes for Xe in channels decorated with paramagnetic centers, we consider a model system using the O_2 molecule as the paramagnetic center. The previously calculated quantum mechanical $Xe@O_2$ hyperfine tensor for various configurations of Xe in the presence of O_2 provides a model for the hyperfine response of Xe atom to the presence of a paramagnetic center. The averaging is carried out using the same grand canonical Monte Carlo methodology as for calculating NMR line shapes for Xe in diamagnetic channels, modified to include the effects of the hyperfine tensor response. We explore the temperature dependence of the Xe line shapes, the dependence on the concentration, and the symmetry of distribution of embedded paramagnetic centers, on the orientation of the paramagnetic center axis with respect to the channel axis, and on the radial distance of the paramagnetic center from the axis of the channel. We predict Xe line shape signatures of the presence and orientation of paramagnetic centers and deduce which tensor elements provide measures of concentration and radial distance of paramagnetic centers from the channel axis. © *2006 American Institute of Physics*. [DOI: 10.1063/1.2338809]

INTRODUCTION

Porous materials are of scientific and technological interest.[1] Recent significant advances in the ability to fabricate new porous solids with ordered structures have resulted in materials with unusual properties and broad applications.[2,3] Some of the new ordered porous materials are paramagnetic or have paramagnetic centers within the pores or channels. For example, inorganic nanotubes can involve high spin complexes,[4] supramolecular networks formed from polyfunctional organic ligands and transition metal ions which form porous coordination polymers or metal-organic frameworks can naturally include metal ions that have unpaired spins;[5–7] anodic alumina membranes can have singly ionized oxygen vacancies (F^+ centers);[8] and of course, any porous channeled structure can be doped with paramagnetic centers at the inside walls where exposed functional groups can be exchanged or functionalized with spin labels or metal ions.

There have been many examples in which Xe NMR has been very useful in probing diamagnetic porous solids.[9–11] Given that Xe atom has an amplified shielding response to its environment, giving rise to a large intermolecular chemical shift range, it has been proposed that Xe NMR would find application in probing paramagnetic channels, where the apparent Xe chemical shift tensor would include not only the usual Xe shielding response but also the contributions coming from its amplified intermolecular hyperfine tensor response to the unpaired spin densities within the channel.[12] When placed in an external magnetic field, the unpaired electron spins of the paramagnetic centers within the sample provide an additional local field at the position of each neighboring nucleus. The magnitude of this local field will determine the additional shift of the NMR signal of any nucleus beyond that of the diamagnetic system. The additional local field at the position of the nucleus is further amplified by spin polarization of the electrons of the Xe atom, so that the Xe nucleus experiences a larger hyperfine shift than would a neutron or ^{3}He nucleus in the same location. Thus, we expect large hyperfine shifts which can provide the basis for the application of ^{129}Xe NMR as an ultrasensitive probe for the detection of the presence and the distribution of paramagnetic centers in the sample. There are experimental reports of large unusual ^{129}Xe chemical shifts in porous materials where paramagnetic centers may be present,[13] but the results were largely unexplained, in part because of lack of model systems for comparison, and in part because of the lack of independent structural information. More recently, a large change in the line shape and a moderate change in the isotropic value of the ^{129}Xe chemical shift was observed for Xe in the hexagonal channels of a molecular crystal of $Co(en)_3Cl_3$ upon replacing the Co^{3+} ion with a Cr^{3+} ion.[12] This is an important and encouraging observation because the architecture and detailed atomic structure of the channels are very nearly the same in the diamagnetic and paramagnetic counterparts.

Our objective is to make predictions of the Xe NMR line shapes for Xe in channels decorated with paramagnetic centers. We aim to investigate the temperature dependence, the dependence on the diameter of the channel, on the number and symmetry of distribution of embedded paramagnetic

[a)]Author to whom correspondence should be addressed. Electronic mail: cjjames@uic.edu

centers per unit cell, and on the orientation of the paramagnetic center axis with respect to the channel axis, using the O_2 molecule as the model paramagnetic center. The quantum mechanical $Xe@O_2$ paramagnetic chemical shift provides the response of Xe atom to the electrons of the paramagnetic center. The averaging will be carried out using a similar grand canonical Monte Carlo (GCMC) methodology as for Xe in diamagnetic channels.[14–16] Using carbon nanotubes as the model architecture for the diamagnetic channel permits the investigation of the Xe line shape dependence on the channel diameter (a) for channel atoms having the same electronic structure and the same channel architecture and (b) at a constant surface density of channel atoms.[17] The temperature dependence of the Xe line shape will be particularly interesting since this will result from a convolution of (a) the temperature dependence of the interaction of a single Xe atom with the channel, (the Xe one-body distribution changes with temperature), (b) the adsorption isotherm (the Xe occupancy changes with temperature and introduces variations in the Xe–Xe contributions to the chemical shift tensor), and (c) the Curie $(1/T)$ behavior of that part of the observed chemical shift arising from the hyperfine tensor.

METHODOLOGY

The model system

We build (using Material Studio 4.0, Accelrys, San Diego, CA) a crystal with an array of carbon nanotubes running along the crystallographic c axis. The diameter of the channel can be varied over a range, without changing the surface density of channel atoms, by choosing different numbers of carbons forming the tube cross section. The carbon nanotubes can be decorated with paramagnetic centers while retaining the essential axial symmetry of the channel by a judicious choice of nanotube size and paramagnetic center positions. We use the O_2 molecule as a model paramagnetic center since the complete set of electronic responses of Xe in the presence of the O_2 molecule have been calculated previously as a function of configuration (R,θ),[18] namely, the Xe shielding response function that is also present for Xe interacting with any diamagnetic molecule, the Xe dipolar hyperfine tensor response, and the spin density at the Xe nucleus arising from the Fermi contact interaction. We will calculate the NMR line shape for Xe occluded in the nanochannels of a polycrystalline material in equilibrium with overhead Xe gas, including diamagnetic shielding terms and hyperfine terms. Since this is only a model system in which we are trying to predict the changes in Xe chemical shifts and line shapes upon doping the nanochannels with paramagnetic centers, we can choose the interactions between the Xe atom and the atoms of the nanotubes to be electronically similar to that of Xe with Ne atoms or with Ar atoms. To start, we will assume that the atoms of our nanotube have the electronic structure of Ne atoms.

Model channels used here are shown in Figs. 1 and 2. We build a supercell that is at least 24 Å on the side (to be able to use energy cutoffs at 12 Å in the minimum image convention). The unit cell, in which all model channels were constructed, was triclinic with all 90° angles and the lattice parameters were 12.00, 12.00, and 8.409 Å, with the channel axis along the crystal c axis. The supercell used in the simulations is $2\times2\times3$ unit cells, and has dimensions 24.00, 24.00, and 25.224 Å. The carbon nanotube chosen for this purpose is a $(n,0)$ zigzag type. We construct channels with different diameters. In the first type of channel architecture, the C–C nucleus-to-nucleus distance across the tube is 9.4 Å, which we use for all models except models D and H. For the smaller diameter channels which we use in model D, the nucleus-to-nucleus distance across the tube is 7.1 Å; for the larger diameter channels in model H it is 11.8 Å. We introduce dummy atoms into the crystal at strategic symmetry-dictated positions so as to prevent the Xe atoms from being created in interstitial positions between nanotubes.

Model systems are constructed by replacing C–C units with O_2 molecules in various ways so as to investigate the Xe line shape signatures associated with the orientation of the axis of the paramagnetic center relative to the axis of the channel and the concentration and distribution of paramagnetic centers. In model A the O_2 molecules are arranged so as to have four equally spaced O_2 molecules girding the channel, essentially replacing four C–C units, except that the positions are adjusted so that the O atoms are on the same line as C–C would have been, but placed closer together so as to have the proper 1.2074 Å distance appropriate for an O_2 molecule rather than the 1.424 Å of the C–C bond. Two views are shown for model A in Fig. 1: perpendicular to the c axis and looking down the c direction. This we call the parallel arrangement of paramagnetic centers, where the axis of the paramagnetic center is parallel to the channel axis. Model B is constructed in a similar fashion as model A, and this has the same concentration of paramagnetic centers, and the same parallel orientation, but the nanotubes have been rotated about the channel axis so as to have a different distribution of paramagnetic centers within the simulation box, while keeping all other parameters the same as in model A. A comparison of model A with model B will provide an indication of whether, for the same concentration of paramagnetic centers, and for the same orientation of paramagnetic center axis relative to the channel axis, the Xe atom can distinguish between different distributions of centers in the solid.

To investigate the influence on the Xe line shape arising from the orientation of the axis of the paramagnetic center relative to the channel axis, we introduce model C. We replace the C–C units with O_2 molecules, this time with one O in the center of the C–C line, such that the O–O bond is projecting outside the nanotube, as shown in Fig. 1. This has the same concentration and the same distribution of paramagnetic centers as model B; only the orientation of the paramagnetic centers relative to the channel axis is different from model B. We call this model C our perpendicular orientation. In order to investigate the effect of the diameter of the channel, or the distance of the paramagnetic centers from the axis of the channel, we introduce models D and H, shown in Fig. 1; both have the same parallel orientation of paramagnetic centers as model B; models D and H have, respectively, smaller and larger diameter channels compared to model B, with three and five O_2 molecules arranged in a ring at each

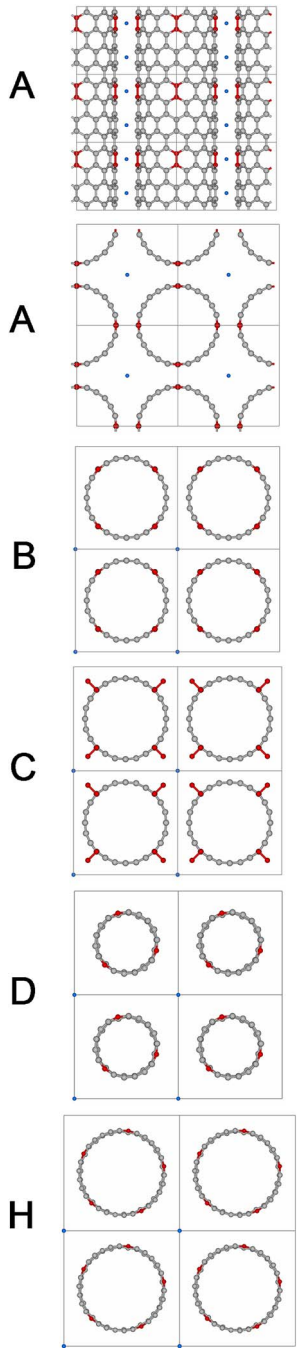

FIG. 1. The supercells constructed for model systems used in this work (the simulation box). All have the same paramagnet to framework atom ratio. The dark atoms are the C–C units in the original carbon nanotube which have been replaced by O_2; the dots are dummy atoms placed between nanotubes to prevent the Xe atoms from being created in interstitial positions. The lines delineate the unit cells. All views, except for model A are looking down the c axis of the crystal. The side view of model A shows the O_2-doping pattern (one ring per unit cell). The four O_2 molecules are arranged in a ring so as to have the axis of the paramagnetic center parallel to the channel axis. All the models shown in this figure have the O_2-doping pattern seen in the side view of model A, i.e., one ring per unit cell. Model B has the same arrangement, and the same distribution within the channel as in model A, but the distribution within the crystal is different from model A. Model C has the same distribution of paramagnetic centers as model B, but the axes of the paramagnetic centers are perpendicular to the channel axis. Model D channels have smaller diameter, and the same parallel orientation of paramagnetic centers as model B; there are three O_2 molecules arranged in a ring. Model H channels have larger diameters, and the same parallel orientation of paramagnetic centers as model B; there are five O_2 molecules arranged in a ring.

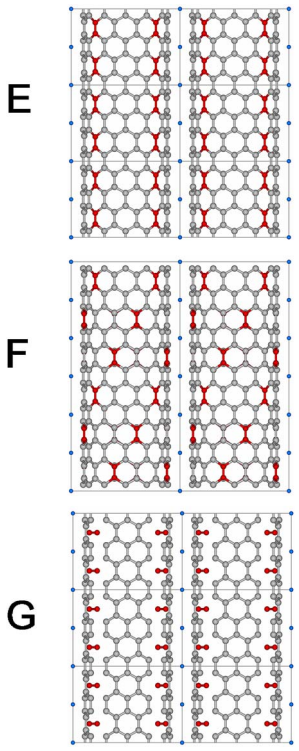

FIG. 2. The supercells for the model systems which have twice the concentration of paramagnetic centers compared to corresponding models in Fig. 1. All have four O_2 molecules arranged in a ring. Model E has the same parallel arrangement of paramagnetic centers as model B, with the four O_2 molecules stacked vertically every level rather than every other level. Model F has the same parallel arrangement of paramagnetic centers as model E, but the positions of the four O_2 units rotate at each level producing a helical pattern. Model G has the same perpendicular orientation of paramagnetic centers as model C.

level, respectively, so as to maintain the same surface density of paramagnetic centers as in model B. All three models have the same concentration of paramagnets in the channel; the O to C atom ratio is 1:11 in each case. By keeping these variables constant, we can isolate the effect of the radial distance of the paramagnetic center from the axis of the channel on the Xe line shape characteristics.

In order to investigate the effect of the concentration of paramagnetic centers on the Xe line shapes, we introduce three models (Fig. 2) which have double the concentration of paramagnets compared to the models shown in Fig. 1, that is, O:C ratio is 2:11. Model E has the same parallel orientation of the four O_2 molecules in a ring as in model B, but this time the O_2 molecules are found at every level, rather than every other level along the axis of the nanotube, so that the concentration of paramagnetic centers is doubled. Similarly, model G has the doubled concentration of paramagnetic centers compared to model C, while retaining the perpendicular orientation of the paramagnetic center relative to the channel axis. In a further investigation of the effect of distribution of paramagnetic centers, we introduce model F, which has the same orientation of O_2 molecules parallel to the channel axis, and the same concentration of paramagnetic centers, i.e., four molecules in a ring at every level just as in model E, but with a different distribution of centers within the channel, as seen in Fig. 2. In model F the positions of the four O_2 molecules

rotate from level to level so that a helical array of O_2 molecules is presented to the Xe atom. At each level the distribution of paramagnetic centers in the solid is the same.

The Xe shielding response and the hyperfine response functions

The Xe response to the paramagnetic centers embedded in the channel is included in the calculations of Xe NMR line shapes by producing Xe line shapes in the same fashion as for diamagnetic channels, but with added "shielding-like" terms coming from the hyperfine tensor of $Xe@O_2$. For these simulations, we use the diamagnetic shielding tensor plus the full hyperfine tensor in $Xe@O_2$, i.e., both the isotropic Fermi contribution and the traceless anisotropic (dipolar) part, which we had previously calculated at the DFT/B3LYP level.[18]

The diamagnetic shielding response tensor from interactions of Xe with the channel atoms

To calculate line shapes of Xe, we require the shielding response in an external magnetic field ($\boldsymbol{B}_0$) oriented in a particular direction (Θ, ϕ). Such a response can be calculated by the following relation:[19]

$$\begin{aligned}\sigma_{B0}(\Theta,\phi) = {} & \sigma_{XX}\sin^2\Theta\cos^2\phi + \sigma_{YY}\sin^2\Theta\sin^2\phi \\ & + \sigma_{ZZ}\cos^2\Theta + \tfrac{1}{2}(\sigma_{XY}+\sigma_{YX})\sin^2\Theta\sin 2\phi \\ & + \tfrac{1}{2}(\sigma_{XZ}+\sigma_{ZX})\sin 2\Theta\cos\phi \\ & + \tfrac{1}{2}(\sigma_{YZ}+\sigma_{ZY})\sin 2\Theta\sin\phi, \end{aligned} \tag{1}$$

provided the components of the shielding of the Xe atom in the laboratory frame of our simulation box, σ_{XX}, σ_{YY}, σ_{XY}, etc. are known. The shielding tensor is treated in the *additive* approximation, as in our previous work.[14] For the isotropic shielding, this additivity approximation assumes that the total isotropic shielding can be written as a sum over individual Xe–C contributions, where C is a channel atom. For calculating the anisotropic shielding response of Xe interacting with the channel atoms and the many Xe atoms in the same channel, the form of the additive approximation we use is described as the dimer tensor model.[14] That is, we represent the tensor of an individual Xe at a particular position within the channel by a sum over contributions of Xe–C dimer tensors, as if the Xe shielding tensor can be reconstituted by tensor components from Xe interacting with one channel atom at a time. Using the dimer tensor model, we consider σ_{XX} for Xe in an arbitrary position in the channel to be a sum over contributions to σ_{XX} coming from every Xe-channel atom pair, with the pair taken to be a dimer having a characteristic tensor which is a function of the distance between Xe and the channel atom. For the carbon nanotube, the contribution from each C to the Xe shielding tensor components in the laboratory frame is given by equations of the form

$$\begin{aligned}\sigma_{XX} = {} & [(X_C - X_{Xe})/R_{XeC}]^2\sigma_{\parallel}(Xe-C) \\ & + \{[(Y_C - Y_{Xe})/R_{XeC}]^2 \\ & + [(Z_C - Z_{Xe})/R_{XeC}]^2\}\sigma_{\perp}(Xe-C), \end{aligned} \tag{2a}$$

$$\begin{aligned}\tfrac{1}{2}(\sigma_{XY}+\sigma_{YX}) = {} & [(X_C - X_{Xe})/R_{XeC}][(Y_C - Y_{Xe})/R_{XeC}] \\ & \times\{\sigma_{\parallel}(Xe-C) - \sigma_{\perp}(Xe-C)\}. \end{aligned} \tag{2b}$$

Only the symmetric part of the shielding tensor can be produced in using dimer tensor model. This suffices, since the antisymmetric part contributes to the observed line shape only to second order.

When the dimer tensor model is used, components $\sigma_{\parallel}(Xe-C)$ and $\sigma_{\perp}(Xe-C)$ are assumed to be known from quantum mechanical calculations. In the model system being used for the present work, the atoms of our nanotube are assumed to have the electronic structure of Ne atoms. The contribution to the Xe shielding due to each Ne atom is given by the *ab initio* tensor component functions $(\sigma_{\perp}, \sigma_{\parallel})_{XeNe}$ (evaluated at R_{XeNe}).[20] Line shape calculations require the component along the $\boldsymbol{B}_0$ direction of this shielding at Xe_J due to Ne_i,[14]

$$\sigma_{B0}(\text{due to } XeNe_i) = (\sigma_{\parallel})_{XeNe}\cos^2\gamma + (\sigma_{\perp})_{XeNe}\sin^2\gamma, \tag{3}$$

where γ is the angle between the two vectors $\mathbf{R}_{XeNe}$ oriented at (Θ_i, ϕ_i) relative to the laboratory Z axis, and $\boldsymbol{B}_0$ oriented at (Θ, ϕ) with respect to the laboratory Z axis,

$$\begin{aligned}\cos\gamma = {} & \sin\Theta\cos\phi[(X_C - X_{Xe})/R_{XeC}] \\ & + \sin\Theta\sin\phi[(Y_C - Y_{Xe})/R_{XeC}] \\ & + \cos\Theta[(Z_C - Z_{Xe})/R_{XeC}]. \end{aligned} \tag{4}$$

In the dimer tensor model, the Xe shielding of the Jth Xe atom at position (X_J, Y_J, Z_J) is also calculated by using a summation over the contributions of Xe–Xe dimers, using the *ab initio* XeXe dimer shielding function in each case.[20] The component of the shielding at Xe_J due to Xe_L along the $\boldsymbol{B}_0$ direction is

$$\sigma_{B0}(\text{due to } XeXe_L) = (\sigma_{\parallel})_{XeXe}\cos^2\gamma + (\sigma_{\perp})_{XeXe}\sin^2\gamma, \tag{5}$$

in terms of the coordinates of the Xe_J and Xe_L,

$$\begin{aligned}\cos\gamma = {} & \sin\Theta\cos\phi[(X_L - X_J)/R] \\ & + \sin\Theta\sin\phi[(Y_L - Y_J)/R] \\ & + \cos\Theta[(Z_L - Z_J)/R]. \end{aligned} \tag{6}$$

As in previous work, the dummy atoms which prevent Xe from being created in the interstitial regions between channels are distributed throughout the crystal but do not contribute to the shielding.

The diamagnetic shielding response tensor from the paramagnetic center

The shielding response for Xe interacting with O_2 has been calculated quantum mechanically and the isotropic *ab initio* values at each configuration can be fitted to the following form:

$$\{\sigma_{\rm iso}(R,\theta)-\sigma_{\rm iso}(\infty)\}=\sum_{p=6,{\rm even}}^{12}R^{-p}\sum_{\lambda=0,{\rm even}}^{6}a_{p\lambda}P_\lambda(\cos\,\theta), \tag{7}$$

and each individual *ab initio* shielding tensor component can also be fitted to the same form

$$\{\sigma_{xx}(R,\theta)-\sigma_{xx}(\infty)\}=\sum_{p=6,{\rm even}}^{12}R^{-p}\sum_{\lambda=0,{\rm even}}^{6}c_{p\lambda}P_\lambda(\cos\,\theta). \tag{8}$$

Using these natural coordinates of the $Xe@O_2$ molecular system offers the advantage of a much closer fit to the *ab initio* values than is possible with site-site fitting (distances only). Note that the *xx*, *yy*, *zz*, *xz*, … tensor components in Eq. (8) are defined in the molecular frame of the $Xe–O_2$ complex, as specified by the input coordinates used in the electronic properties calculations. In the simulation, the R and the θ values are determined *in situ* in the channel from the laboratory coordinates of the Xe, O_1, and O_2 atoms in the simulation box. From these (R,θ) molecular coordinates, the isotropic shielding $\{\sigma_{\rm iso}(R,\theta)-\sigma_{\rm iso}(\infty)\}$ values are regenerated by the coefficients $a_{p\lambda}$. Similarly, for these (R,θ) values, the quantum-mechanically calculated shielding tensor values σ_{xx}, etc. are regenerated from the coefficients $c_{p\lambda}$. The elements of the required tensor $\sigma_{XX},\ldots$ in the laboratory frame of the simulation box are generated from the tensors in the molecular frame, $\sigma_{xx},\ldots$, by making a transformation from molecular frame of the $Xe@O_2$ complex to the laboratory frame of the simulation box for each Xe and each O–O unit, for every accepted Monte Carlo configuration, as follows:

$$\sigma_{(XYZ)}=C^T\sigma_{(xyz)}C. \tag{9}$$

From the $\sigma_{XX},\ldots$ values, Eq. (1) provides the shielding component along $\boldsymbol{B}_0$ that is required for the line shape calculations. The transformation coefficients C are given in the Supporting Information.[21]

The Fermi contact contribution from the paramagnetic center

The Fermi contact part, which has been calculated as a spin density, contributes to the apparent chemical shift. The spin density, in units of $\rm bohr^{-3}$, can be written as

$$\{\rho(R,\theta)-\rho(\infty)\}=\sum_{p=6,{\rm even}}^{12}R^{-p}\sum_{\lambda=0,{\rm even}}^{6}b_{p\lambda}P_\lambda(\cos\,\theta), \tag{10}$$

where, we have found the coefficients $b_{p\lambda}$ for $p=6,\ldots,12$, (even), $\lambda=0,\ldots,6$, (even), by fitting the spin densities at various configurations (R,θ) for Xe in the molecular frame of O_2. The isotropic Fermi hyperfine contribution which appears equivalent to a contribution to nuclear shielding at the Xe nucleus is given by[22,23]

$$\left(\frac{\Delta B}{B_0}\right)(T)_{\rm Fermi}=\sigma_{\rm Fermi}(T)=-[S(S+1)8\pi g_e^2\mu_B^2/9kT]\{\rho(R,\theta)-\rho(\infty)\}, \tag{11}$$

where, $\{\rho(R,\theta)-\rho(\infty)\}$ is the spin density, normalized to 1, relative to that for infinite separation (the latter taken from a counterpoint calculation). We find that the GAUSSIAN 98 output of "spin density" is normalized not to 1 but to $2S$, that is, the output is $\rho_{\rm Gaussian}=2S\rho(R,\theta)$ in units of $\rm bohr^{-3}$. Therefore, to obtain the contribution to the shielding at temperature T, we need

$$\sigma_{\rm Fermi}(T)=-[(S+1)4\pi g_e^2\mu_B^2/9kT]\rho_{\rm Gaussian}, \tag{12}$$

where $(S+1)=2$ for $Xe@O_2$, and the counterpoise correction $\rho_{\rm Gaussian}(\infty)$ is negligibly small. In the calculations of the contribution to the Xe NMR line shape the component of the shielding along the $\boldsymbol{B}_0$ direction coming from the Fermi contribution is the same amount for any direction of $\boldsymbol{B}_0$, since the Fermi contact term is entirely isotropic.

The hyperfine dipolar contribution from the paramagnetic center

We handle the dipolar part of the hyperfine tensor as follows: The term in the Hamiltonian is[23]

$$\boldsymbol{A}_{\rm Xe,dipolar}\cdot\boldsymbol{I}=2\hbar\mu_B\gamma_{\rm Xe}\sum_i\left\{\frac{3(r_i\cdot s_i)(r_i\cdot I)}{r_i^5}-\frac{s_i\cdot I}{r_i^3}\right\}. \tag{13}$$

The ith electron's vector position r_i is in the x, y, z molecule-fixed axis system, and in general, of course, the $\boldsymbol{B}_0$ direction $\hat{k}$ does not lie along the z axis. This gives rise to a shielding-like term, a dimensionless quantity

$$\langle\Delta B/B_0\rangle=(1/\hbar\gamma_{\rm Xe}B_0)\langle\boldsymbol{A}_{\rm Xe}\rangle\cdot\hat{k}, \tag{14}$$

where the average over thermally populated states is indicated by $\langle\,\rangle$, and where $\boldsymbol{B}_0$ has a fixed orientation $\hat{k}$ with respect to the axis system of the complex. Thus, we need the tensor quantity $\sigma_{\alpha\beta\ \rm dipolar}$

$$\sigma_{\alpha\beta\ \rm dipolar}=\left(\frac{\Delta B}{B_0}\right)_{\alpha,\beta}=-[S(S+1)g_e^2\mu_B^2/3kT]\left\langle\sum_i\left\{\frac{3r_{i\alpha}r_{i\beta}-1r_i^2}{r_i^5}\right\}\right\rangle_{\rm spin}. \tag{15}$$

As in the Fermi contact term, the subscript "spin" implies averaging over the unpaired spin density normalized to unity in Eq. (15). Comparing this with $\sigma_{\rm Fermi}$, we note that the constant factors differ from those in the Fermi term only in that the dipolar term has no $(8\pi/3)$ factor. The dipolar hyperfine tensor, a traceless tensor, is reported by GAUSSIAN 98 as either the *xx*, *yy*, *zz*, *xz* components in the molecular frame, or as principal components B_{aa}, B_{bb}, B_{cc}, also in units of $\rm bohr^{-3}$. In the molecule-fixed axis system

$$\sigma_{\alpha\beta\ \mathrm{dipolar}} = -[(S+1)g_e^2\mu_B^2/6kT]B_{\alpha\beta,\mathrm{Gaussian}}$$
$$\alpha,\beta = x,y,z. \tag{16}$$

For Xe line shape calculations, we need to be able to calculate, for arbitrary configurations of $Xe@O_2$, the component along $\boldsymbol{B}_0$ of the general tensor $\sigma_{\alpha\beta,\mathrm{dipolar}}$, in Eq. (16).

Each of the B tensor elements appear to have similar symmetry properties with configurations (R,θ) as does the isotropic Fermi contact hyperfine spin densities in $Xe@O_2$. We therefore represent the entire complement of quantum mechanically calculated values by fitting each of the B_{xx}, B_{yy}, B_{zz}, B_{xz} dipolar components to functions of the type

$$\{B_{xx}(R,\theta) - B_{xx}(\infty)\} = \sum_{p=6,\mathrm{even}}^{12} R^{-p} \sum_{\lambda=0,\mathrm{even}}^{6} d_{p\lambda}P_\lambda(\cos\theta), \tag{17}$$

to provide the coefficients $d_{p\lambda}$ of the above interpolating function which describes the dipolar components. Inside the simulation, we resurrect the values of the B tensor for every $Xe@O_2$ using Eq. (17). We then carry out the matrix transformation of the local $Xe@O_2$ dipolar components to the B tensor components in the laboratory frame of the simulation box

$$B_{(XYZ)} = C^T B_{(xyz)} C \tag{18}$$

using the same transformation coefficients as for the diamagnetic shielding. After this, we find the contribution to the shielding tensor component arising from the dipolar tensor

$$\sigma_{XX,\mathrm{dipolar}} = -[(S+1)g_e^2\mu_B^2/6kT]B_{XX}. \tag{19}$$

From these values, Eq. (1) provides the component along $\boldsymbol{B}_0$ for the line shape calculations.

The bulk magnetic susceptibility contribution

For direct comparison with experiments, the predicted Xe line shape has to include the contributions of the bulk magnetic susceptibility to the line shape. Since this contribution is determined by the boundaries which define the shape of the particular experimental sample under observation, we do not include this factor in the chemical shift calculations reported here.

The potential functions needed for averaging

The potential function for Xe@nanotube interactions is simplified for our model system. There are previous GCMC simulations of Xe in carbon nanotubes by Yates and co-workers.[24] They used a Lennard-Jones potential for Xe–Xe (r_0=4.1 Å and ε/k_B=221 K)[25] and an anisotropic (6) and (12) Xe-graphitic potential[26] for the Xe–C interactions in terms of $R_{\mathrm{Xe–C}}$ and the angle between the tube surface normal and the line connecting Xe with a carbon atom. Since the simulation of actual Xe line shapes in carbon nanotubes is not the objective of this work, we do not need to use a graphitic potential at this stage. For this model system of nanochannels decorated with paramagnetic centers, we use the shielding response function σ(Xe–Ne) for the Xe-channel shielding response, rather than a Xe-graphitic shielding response. For consistency, we use the Maitland–Smith fit to the best empirical V(Xe–Ne) for the potential energy function for Xe-channel atom.[14]

The potential function for $Xe@O_2$ interactions from Aquilanti *et al.*[27] is the best available empirical potential, which we used for averaging the shielding in gas phase mixtures of Xe and O_2.[18] For the present GCMC simulations, we fitted this $Xe–O_2$ potential function to a sum, $V(Xe–O_1)+V(Xe–O_2)$, each one in the Maitland–Smith form, so that the nature of the Xe-paramagnetic center intermolecular interactions is qualitatively similar to that between Xe and the diamagnetic channel atoms.

The Xe–Xe interaction potential is the same one we have used for our previous work, a Maitland–Smith form fitted to reproduce the best empirical potential for Xe–Xe from Aziz and Slaman.[28]

RESULTS

The way in which the Xe line shapes change with occupancy is, of course, of interest in practical samples of channels with paramagnetic centers. However, for the first part of this investigation, we are interested in the line shape contribution arising explicitly from the interaction of Xe with the paramagnetic centers. Thus, we will display almost exclusively the results of the line shapes that are obtained in the limit of zero Xe occupancy. This comes out directly from the simulations since the Xe-channel contributions to the line shapes are binned separately from the Xe–Xe contributions and the total line shape. Also, we carried out calculations for three temperatures (300, 250, and 200 K) in every case because the hyperfine contributions to the line shape have the intrinsic $(1/T)$ dependence, in addition to any temperature dependence that arises from temperature-dependent Xe one-body distribution functions. All our calculations are for the nuclear magnetic shielding tensor σ. In the established convention, the span Ω is defined as $\sigma_{33}-\sigma_{11}$, where the principal components of the tensor are in the order $\sigma_{33}>\sigma_{22}>\sigma_{11}$.[29] The accurate definition of the NMR chemical shift is $\delta=(\sigma_{\mathrm{ref}}-\sigma)/(1-\sigma_{\mathrm{ref}})$. Here we use isolated Xe atom as our reference. If we neglect the absolute shielding of Xe atom (0.006) compared to 1.0, then the experimental $(\delta_{\mathrm{larger}}-\delta_{\mathrm{smaller}})$ is approximately equal to the span and the experimental chemical shift is approximately equal to $(\sigma_{\mathrm{ref}}-\sigma)$. For axially symmetric average chemical shift tensors, for convenience and clarity, we retain the older convention of the parallel and perpendicular components, $\delta_\parallel$ and $\delta_\perp$.

In the simulations, the Xe chemical shift components along B_0 are calculated at orientations of the magnetic field sampled uniformly in ϕ, $\cos\Theta$ relative to the stationary crystal. With this uniform sampling the correct relative intensities as a function of parts per million can be displayed, as we have done for diamagnetic channels. However, the spans are much greater for the model systems containing paramagnetic centers and the shape obtained from the pattern of a finite number of bars is less pleasing. Therefore, to generate the intensities for a finer grid, the line shapes shown in the figures have been obtained from the average chemical shift tensor components by using the standard formulas involving

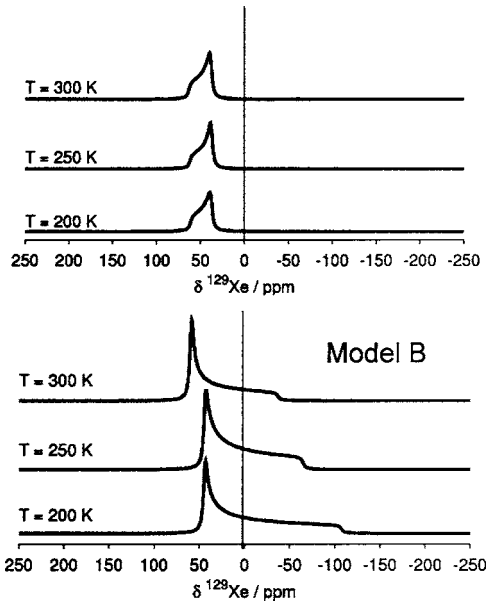

FIG. 3. The Xe line shapes for Xe-channel interactions (in the limit of zero Xe occupancy) at 300, 250, and 200 K in the neon nanotube doped with O_2 in model B (bottom) compared with the Xe line shapes under the same conditions, but with the coefficients of all hyperfine terms zeroed out, i.e., in the absence of hyperfine effects (top).

complete elliptic integrals of the first kind.[30] The overall line shape is generated as sum of Lorentzians as usual, using a broadening parameter of 1–2 ppm.

The diamagnetic channel without the paramagnetic centers

Our results for just the Xe-channel part in model B, where the O–O line of centers are parallel to the channel axis, are shown in Fig. 3. The line shapes for model B are compared here with analogous simulations under all the same conditions except that the hyperfine coefficients have been zeroed out, that is, the O_2 molecules are still in place and their diamagnetic contributions to the shielding are included, but not the hyperfine contributions. The axiality of the chemical shift tensor for a single Xe atom in the presence of paramagnetic centers is opposite to that for Xe in diamagnetic channels. This was found to be the case for all the models used in this work. The chemical shift tensors of a Xe atom in the model diamagnetic channels are summarized in Table III in Supplementary Information.[21]

The concentration of paramagnets

We investigated the effect of the concentration of the paramagnetic centers on the Xe line shape. Model E has the same parallel arrangement as model B, but model E has twice the number of O_2 units per channel compared to model B. Compared to model B in Fig. 3, Fig. 4 shows that the greater concentration of paramagnets in model E has caused $\delta_\parallel$ and $\delta_\perp$ to shift further in opposite directions, leading to a larger width of the NMR powder pattern

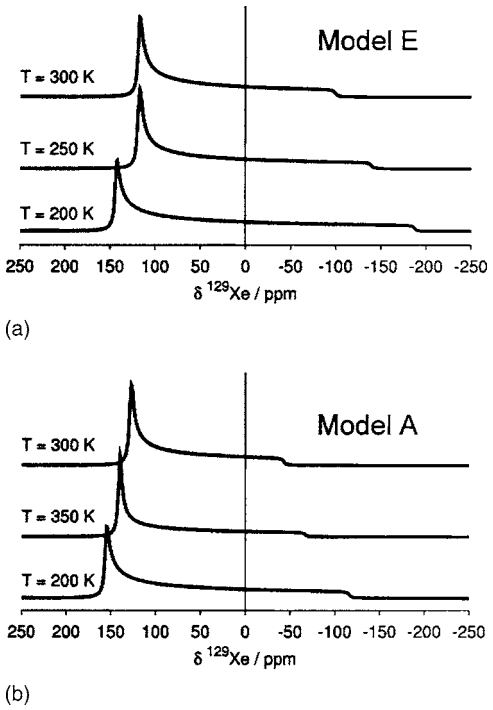

FIG. 4. The effect of concentration and the distribution of paramagnetic centers. (a) Xe line shapes for Xe-channel interactions (in the limit of zero Xe occupancy) at 300, 250, and 200 K in the neon nanotube doped with O_2 in model E (top) which has twice the concentration of paramagnetic centers as model B in Fig. 3. (b) Xe line shapes in model A (bottom) which have the same concentration and arrangement of paramagnetic centers within the channel as model B in Fig. 3, but the distribution of paramagnets in the solid is different.

The orientation of paramagnets

We observed the effect that the orientation of the axis of the paramagnetic centers relative to the axis of the channel has on the Xe line shapes. In Fig. 5 we show the line shapes

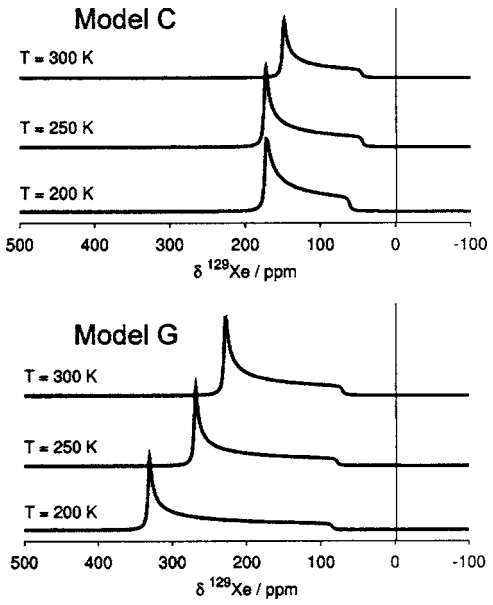

FIG. 5. The axis of the paramagnetic center is perpendicular to the axis of the channel. Line shapes in model C (top) are compared with line shapes in model G which has twice the concentration of paramagnetic centers (bottom).

in model C (perpendicular orientation) which may be compared to model B (parallel orientation) in Fig. 3. All other conditions are the same, namely, the same concentration of paramagnets, and the same distribution in the simulation box; only the orientation of the axes of the paramagnetic centers relative to the channel axis is different. When the axis of the paramagnet is parallel to the channel axis, the hyperfine contribution is largely to $\delta_{\parallel}$ and negative; the hyperfine contribution to $\delta_{\perp}$ is smaller and positive (except in the channel with very small diameter, in which case the entire chemical shift tensor is large negative). On the other hand, when the axis of the paramagnet is perpendicular to the channel axis, the hyperfine contribution is largely to $\delta_{\perp}$ and positive; and the hyperfine contribution to $\delta_{\parallel}$ is also positive and small. We can also compare the line shapes of a Xe atom in model E in Fig. 4 with that in model G in Fig. 5, which is analogous to the model B versus model C comparison, but at twice the concentration of paramagnets in the channel. We can see that the Xe atom can definitely distinguish that the orientation of the paramagnetic centers are different in the two cases.

A consequence of the confinement is that for the perpendicular arrangement, the Xe atom samples the short r values only for θ close to 0°, while for the parallel arrangement, Xe samples the short r values for a wide range of θ values on either side of 90°, but not including small θ. Since the Fermi contact contribution is highly dependent on the orientation of the O_2 axis with respect to the intermolecular axis in the $Xe@O_2$ complex, the isotropic part of the chemical shift tensor arising from the hyperfine interaction is sensitive to the orientation of the O_2 axis with respect to the channel axis.

The distribution of paramagnets within the channel

To discover the sensitivity of the Xe line shapes to the distribution of paramagnetic centers within the channel, we compare models E and F. Both have the same concentration of paramagnets; all are oriented parallel to the axis of the channel. At any z level in the nanotube, the distribution throughout the solid is the same in model F as in model E, but the distribution in the channel is different (see Fig. 2). The difference between the Xe line shapes for a single Xe in the channels of models E and F (not shown) is not great (see the hyperfine chemical shift tensors in Table I). The $\delta_{\parallel}$ response, which is the component that dominates the hyperfine contribution for the parallel arrangement of paramagnets, is governed by the electron distribution in the plane containing the Xe nucleus and perpendicular to the axis of the channel. At a particular Xe position in the channel, the closest O_2 neighbors are essentially the same for both models E and F which leads to very similar $\delta_{\parallel}$ response. The Xe atom sees a difference in the longer range distribution of the paramagnetic centers within the channel, leading to a larger difference in the $\delta_{\perp}$ response and a greater span of the hyperfine contribution in model F than in model E. Xe does discriminate between models E and F, but the differences in the resulting Xe line shape are not profound.

TABLE I. The hyperfine contributions to the Xe chemical shift tensor in each of the model systems.

	300 K				250 K				200 K			
Model	δ_{cc}	δ_{aa}	δ_{bb}	Span	δ_{cc}	δ_{aa}	δ_{bb}	Span	δ_{cc}	δ_{aa}	δ_{bb}	Span
A	−107.3±0.8	87.6±6.7	90.0±4.2	197.3±5.0	−130.5±4.3	100.8±6.7	102.8±4.8	233.4±9.1	−181.0±9.0	116.5±12.3	116.1±9.3	297.5±21.3
B	−100.1±2.6	20.6±9.3	21.8±9.8	122.0±12.5	−129.0±2.8	5.9±7.0	5.9±6.3	134.9±9.1	−169.4±1.2	6.5±12.2	7.5±9.6	176.9±10.8
C	12.2±0.6	100.7±1.8	101.1±1.5	88.8±2.1	14.1±2.6	120.3±4.5	120.1±4.1	106.1±7.1	16.8±2.4	149.7±3.3	149.7±3.0	132.9±5.7
E	−175.3±4.2	67.2±20.6	68.6±19.1	243.9±23.3	−213.1±2.3	68.2±12.2	70.1±13.7	283.1±16.6	−261.5±4.9	95.4±10.3	94.8±6.0	356.9±15.2
G	28.8±3.0	204.8±3.5	204.6±3.7	176.0±6.5	34.7±4.2	245.5±5.2	245.6±4.8	210.9±9.0	44.8±5.4	308.4±7.9	308.7±7.8	264.0±13.2
F	−186.4±3.7	88.2±16.3	87.7±16.9	274.6±20	227.1±4.1	89.0±19.0	91.1±18.4	318.2±22.5	−283.9±4.6	98.9±24	98.7±25	382.9±28.6
D	−508.2±49	−121.8±134	−120.4±131	387.9±180	−645.2±19	−165.1±38	−157.8±43	487.4±62	−818.3±51.5	−273.1±285	−267±273	551.3±324
H	−85.1±2.9	28.8±7.3	33.8±4.7	118.7±7.6	−107.1±2.1	36.9±6.2	39.2±8.2	146.3±10.3	−143.7±3.4	27.2±16.4	31.1±14.0	174.8±17.4

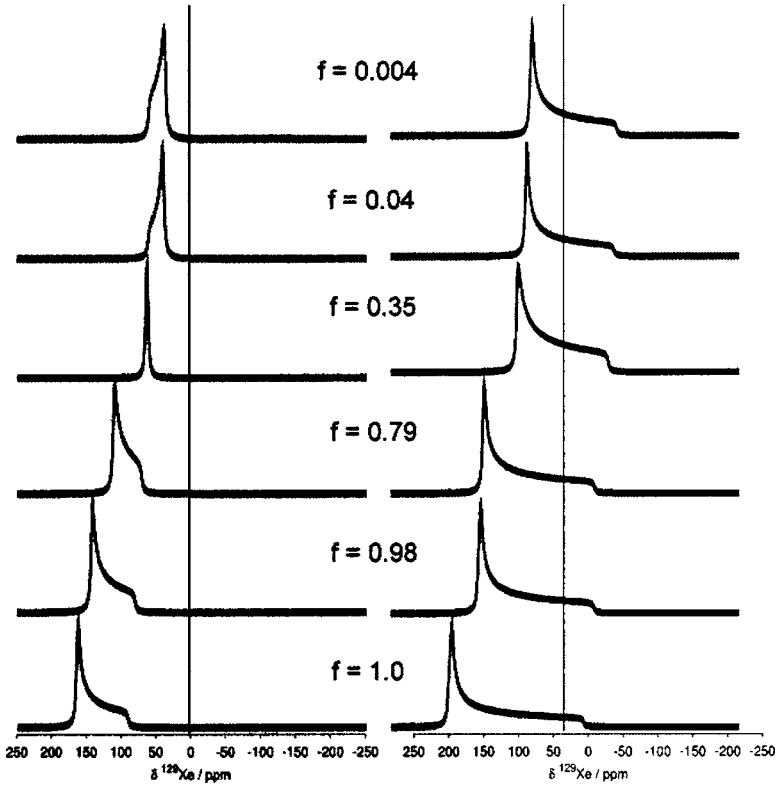

FIG. 6. The Xe line shapes as a function of Xe occupancy. Xe line shapes in the neon nanotube doped with O_2 in model B at 250 K (right) are compared with the line shapes under the same conditions, but with the coefficients of all hyperfine terms zeroed out, i.e., in the absence of hyperfine effects (left). The fractional occupancy $f=\langle N\rangle/\langle N\rangle_{\max}$.

The distribution of paramagnets in the solid

The structure of each channel in model B is the same as in model A, yet the difference between line shapes in model B (Fig. 3) and model A (Fig. 4) is dramatic. The only difference in conditions between the two systems is the distribution of the paramagnetic centers in the crystal: model A has nanotubes rotated with respect to each other such that the O_2 molecules of two adjacent nanotubes are in back-to-back arrangements, with the O_2 from the neighbor channel reinforcing the effects of the O_2 within the same channel as the Xe. This dramatic difference between the Xe line shapes in models A and B originates from the strong dependence of the hyperfine tensor on the angle θ between the Xe-to-O_2 vector and the O–O axis in Xe@O_2. This is not a unique feature of the O_2 system, of course; spin density distributions in most paramagnetic species are highly directional, whether the species is O_2, or a transition metal ion, or an organic free radical. Each spin system has its unique spin density distribution symmetry. The arrangement of the paramagnetic centers in the solid is a characteristic feature of the crystal structure in ordered systems. Thus, we have shown that the Xe atom can differentiate between different crystal structures (polymorphs) of paramagnetic substances.

Xe occupancy

With increasing Xe occupancy of the nanochannel, the Xe line shapes change systematically because of the increasing contributions of the Xe–Xe interactions. The architecture of the channel determines the Xe–Xe one-body distribution functions as the occupancy increases. In fact, the Xe–Xe contributions to the observed average Xe chemical shift tensors are a more sensitive measure of the architecture of the channel, the symmetry of the channel cross section, and the diameter of the channel, than is the chemical shift tensor in the limit of zero occupancy in diamagnetic channels. This is so because the Xe–Xe interactions amplify the shielding signatures which are the effects of confinement by an internal wall of particular shape and corrugation. For the most part, the Xe-channel contributions to the Xe chemical shift tensor (and thus the line shape) change only slightly as the Xe occupancy increases. The Xe–Xe contributions which increase $\delta_\perp$ upon increasing Xe occupancy provide the changes in line shape in both diamagnetic and paramagnetic channels. Since the channel with paramagnetic centers has a different signature line shape in the limit of zero occupancy than does the diamagnetic channel, the way in which the Xe channel and the Xe–Xe combine can lead to rather unique line shape signatures with increasing Xe occupancy. We show one such example in Fig. 6 for Xe in model B. Here the diamagnetic channel line shapes (with the hyperfine coefficients zeroed out) are shown on the left half of the figure. The Xe interactions with the walls are only slightly affected by the presence of the other Xe atoms (unless the occupancy becomes extremely high). At nearly zero occupancy of a diamagnetic channel, $\delta_\parallel > \delta_\perp$. With increasing Xe occupancy, the increasing positive Xe–Xe contributions to the chemical shift lead to larger positive $\delta_\perp$ values. Thus, the Xe line shape in the diamagnetic channel eventually passes through the point of equality of $\delta_\parallel$ and $\delta_\perp$, at which point the line shape looks like that of an isotropic system, and then changes axiality as $\delta_\perp$ exceeds $\delta_\parallel$. For diamagnetic channels of nearly circular cross section, a plot of the tensor components with increasing occupancy usually gives a zero slope characteristic of the $\delta_\parallel$ component along the axis of the channel, and a positive slope for the $\delta_\perp$ component. On the other hand, a single Xe atom

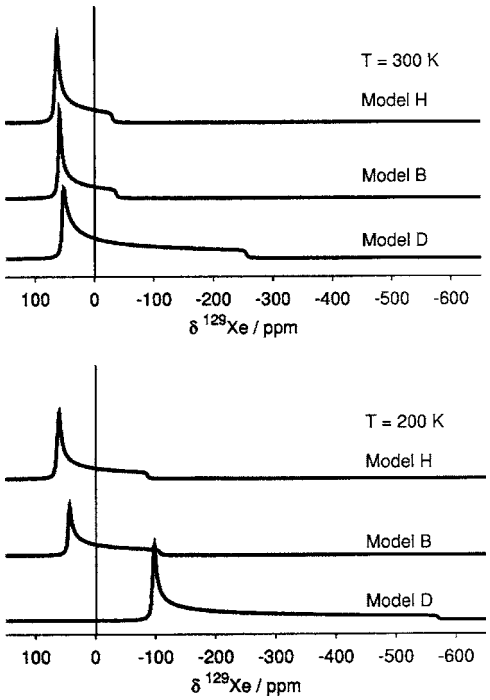

FIG. 7. The effect of the channel diameter. The Xe line shapes for Xe-channel interactions (in the limit of zero Xe occupancy) are compared in the O_2-doped neon nanotubes of increasing diameter in models H, B, and D at 300 (top) and at 200 K (bottom).

in channels containing paramagnetic centers starts out with $\delta_\perp > \delta_\parallel$. With increasing occupancy, the component along the axis of the channel remains at nearly zero slope whereas the perpendicular component has positive slope; thus, the two components diverge with increasing occupancy and never pass through the isotropic-looking line shape. This is indeed what we find in Fig. 6.

The average distance from the paramagnet

Finally, we investigate the ability of Xe to inform on the average distance of the paramagnetic centers from the center of the channel. In this comparison of Xe line shapes in three channels of various diameters, we arrange to keep the surface density of paramagnets the same and maintain the same concentration of paramagnets in the channel at a constant O to C atom ratio of 1:11. The orientation of the paramagnets relative to the axis of the channel is the same. The structural difference is that the diameter of the channel in model D is smaller (in model H, larger) than in model B. The effect of channel radius on Xe line shapes in diamagnetic channels is discussed elsewhere.[17] The smaller channel permits the Xe to be found at shorter distances from the wall atoms, thus weighting the stronger response at short distances more heavily in the average for the Xe-channel atom interactions as well as for the Xe-paramagnet interactions. Shorter average distances permit greater Xe shielding response and also greater hyperfine response. Both the diamagnetic and the paramagnetic channels show smaller Xe chemical shift responses in model H than the channel in models B and D. In Fig. 7 we show the differences in Xe line shapes as the channel diameters are varied, by comparing at the same temperature the line shapes for Xe in the channels of increasing diameter in models D, B, and H at 300 and 200 K. Since other factors (concentration, orientation, and surface density of paramagnets) are identical in all three channels, the differences in Xe line shapes must be a direct consequence of the radial distance of the paramagnetic centers from the axis of the channel. In channels of smaller diameter, the highest probability Xe positions are close to the axis of the channel, as in models D and B, whereas in the channel with the largest cross section (model H), the Xe one-body distribution resembles a cylindrical shell concentric with the channel.[17] For this reason, there is only a small difference between models H and B at 300 K, while model D is markedly different. The progression in line shape, corresponding to the decrease in channel diameter and concomitant decrease in radial distance between the axis of the channel and the paramagnet, is clearly seen in Fig. 7. As the radial distance decreases in going from models H to B to D, shorter distances move the entire Xe line shape toward more negative chemical shifts, and increase the span at the same time, but the most pronounced effect is on $\delta_\parallel$. The hyperfine contributions to the chemical shift tensor change algebraically monotonically with decreasing radius of the channel in going from models H to B to D, as seen in Table I. At the lower temperature, the effect of the decrease in radial distance on the Xe line shape is more pronounced as the contribution for the hyperfine tensor becomes more dominant due to its $1/T$ dependence.

TABLE II. The Fermi contact contributions to the isotropic Xe chemical shift in each of the model systems.

Model	300 K	250 K	200 K
A	30.7±2.5	33.0±4.3	28.1±9
B	−15.1±7.3	−34.5±4.6	−44.3±7.7
C	14.3±0.5	16.6±4.6	19.8±2.2
E	−4.5±15.6	−15.2±10	−11.0±7
G	32.9±3.2	39.6±4.1	50.8±5.8
F	2.2±12.4	−9.9±14	−21.9±19.2
D	−216±103	−281±29	−402±203
H	−2.9±3.7	−4.6±4.9	−21.5±10.7

The isotropic chemical shift

The hyperfine contributions to the Xe chemical shift tensors in each of the model systems are given in Tables I and II. The isotropic shift arising from the Fermi contact interaction is over and above that present in diamagnetic channels. This can have either sign. As we can see in Table II, the isotropic Fermi shift is sensitive to the distribution and orientation of the paramagnetic centers. This additional isotropic shift arising from paramagnetic centers algebraically decreases as the temperature decreases, when the axis of the paramagnetic center is *parallel* to that of the channel axis. On the other hand, when the axis of the paramagnetic center is *perpendicular* to the channel axis, the additional isotropic shift is in the direction of larger positive chemical shifts with decreasing temperature.

SUMMARY OF Xe LINE SHAPE SIGNATURES

We have considered various characteristics of a porous solid decorated with paramagnetic centers: concentration of paramagnetic centers, orientation of the axis of the paramagnetic center relative to the axis of the channel, distribution of the paramagnetic centers in the solid, and the distance of the paramagnetic centers from the axis of the channel. We have constructed model systems to illustrate the differences in Xe line shapes that could occur when each one of these characteristics is changed while keeping the others constant. Our results indicate that Xe line shapes can distinguish between various concentrations, distributions, and distances of paramagnetic centers from the channel axis, and orientations of the paramagnet axis relative to the channel axis. We have also found that the explicit dependence of the hyperfine tensor response at Xe on $(1/T)$, which serves as an amplifying factor at low temperatures, can be used to advantage. The large changes that occur in the hyperfine contributions to the observed line shape permits the separation of the paramagnetic contributions from those arising in the standard diamagnetic channels by taking Xe NMR spectra at lower temperatures.

For Xe in one-dimensional diamagnetic channels (channels running along a single direction of the unit cell), it is possible to infer, directly from signature line shapes obtained in polycrystalline materials, some information about the nature of the channels. The number of singularities in the high-Xe-loading line shapes clearly indicates the aspect ratio of the cross section of the channel; two singularities correspond to a nearly circular channel cross section, three singularities point to an elliptical channel.[14] The constancy of one of the tensor components in the line shape is a clear indication that the channel diameter does not permit two Xe atoms to pass each other in the channel.[14,15] A significant change of the tensor component along the channel axis with increasing occupancy is a signature of a channel cross section large enough to permit $XeXe_2$ groupings in the channels at high Xe occupancy to achieve Xe–Xe–Xe angles smaller than 150°–180°.[31] A linear behavior of each tensor component with average occupancy (Xe atoms per unit cell) is a clear indication of some orderly arrangement of Xe atoms within the channel, as when the Xe is of the correct diameter to sit in register with energy-favorable sites along the internal walls.[32] When the sites are too close together, the Xe is unable to do this. When the cross section of the channel is not uniform throughout, but rather larger and smaller as the Xe goes up the channel, then with the significant probability that two Xe atoms can be in the same cross sectional plane in the channel, a definite nonlinear behavior of tensor components with average occupancy can be expected.[33] When Xe can sample more than one channel system in the crystal (intersecting channels), then three singularities may be expected in both near-zero occupancy and high occupancy line shapes. These are Xe line shape signatures of the architectural characteristics of diamagnetic channels that have been discovered via a combination of experiments and grand canonical Monte Carlo simulations.

Can we infer channel characteristics analogous to the earlier findings directly from the NMR line shapes for Xe in channels containing paramagnetic centers? That is, what does the observed Xe line shape directly tell us about the channel system? From the simulations in the present work, we find several useful signatures for polycrystalline material containing one-dimensional channels doped with paramagnetic centers possessing spin density distributions of spatial symmetry similar to O_2.

(1) By itself, the change in sign of the axiality of the Xe chemical shift tensor at near-zero occupancy of the channel is a signature of the *presence* of paramagnetic centers. For diamagnetic systems, $\delta_\perp < \delta_\parallel$; whereas, we find always $\delta_\perp > \delta_\parallel$ for channels containing paramagnetic centers for any concentration, distribution, or orientation of the paramagnetic systems.

(2) Another unequivocal signature of the *presence* of paramagnetic centers in the channel is the divergence of the individual components from each other as the Xe occupancy increases; that is, the span increases monotonically with increasing occupancy. This is in contrast to the behavior of Xe line shapes commonly found in diamagnetic channels, which exhibit crossing over of $\delta_\parallel$ with $\delta_\perp$, the span decreasing with increasing occupancy, then increasing again, with the Xe line shapes exhibiting an isotropic-like line shape at some particular occupancy where the $\delta_\parallel$ happens to coincide with $\delta_\perp$.

(3) A third unequivocal signature of the *presence* of paramagnetic centers is the observation that $\delta_\parallel$ moves to more negative chemical shifts as the temperature decreases at low Xe occupancy. This temperature behavior is *opposite* to the behavior of the Xe chemical shift tensor in diamagnetic channels, where $\delta_\parallel$ usually moves to more positive chemical shifts with decreasing temperature at a fixed occupancy; and if the Xe occupancy is also increasing with decreasing temperature as happens in continuous flow hyperpolarized Xe experiments, the change of $\delta_\parallel$ to more positive chemical shifts with decreasing temperature is even more pronounced in purely diamagnetic channels.

(4) The *orientation* of the axis of the paramagnetic centers with respect to the channel axis has a $\delta_\parallel$ signature at low Xe occupancy: When the axis of the paramagnetic center is parallel to the axis of the channel, the component of the Xe chemical shift tensor along the axis of the channel, $\delta_\parallel$, is *negative*. On the other hand, if the axis of the paramagnetic center is perpendicular to the axis of the channel, $\delta_\parallel$ is *positive*, that is, the same sign as for diamagnetic systems. This comes about because when the axis of the paramagnet is parallel to the channel axis, the hyperfine contribution is nearly all $\delta_\parallel$ which is unequivocally negative, as can be seen in Table I. On the other hand, when the axis of the paramagnet is perpendicular to the channel axis, the hyperfine contribution is nearly all $\delta_\perp$ which is unequivocally positive. When the Xe atom has a very large shielding response from the diamagnetic channel (such as when the channel diameter is quite small), the question arises, will the $\delta_\parallel < 0$ arising from the hyperfine part alone be sufficient to overwhelm the large positive $\delta_\parallel$ of the diamagnetic part of the channel? For a small channel diameter, we expect and find unequivocally in Fig. 7 that $\delta_\parallel < 0$ arising from the hyperfine part alone is also larger negative due to more intimate interactions at

shorter average distances from paramagnetic centers, and dominates $\delta_{\|}$ especially at low temperatures. Thus, this signature should be fairly robust, provided the paramagnets are at the channel walls rather than located in remote internanotube regions.

(5) The *orientation* of the axis of the paramagnetic centers with respect to the channel axis also has a signature in the temperature dependence of one of the components in the limit of very low occupancy: When the axis of the paramagnetic center is parallel to the axis of the channel, the Xe chemical shift tensor component along the axis of the channel, $\delta_{\|}$, moves to more negative chemical shifts as the temperature decreases (and the $\delta_{\perp}$ component also moves toward more negative chemical shifts). On the other hand, when the axis of the paramagnetic centers is perpendicular to the axis of the channel, the Xe chemical shift tensor component perpendicular to the axis of the channel, $\delta_{\perp}$ moves to larger positive chemical shifts as the temperature decreases (while the $\delta_{\|}$ component moves to somewhat larger positive chemical shifts). In fact, when there is any doubt at all, taking measurements at lower temperatures will undoubtedly resolve any ambiguities, because of the steep intrinsic $1/T$ dependence of the hyperfine tensor.

(6) Relative information about the *concentration* of paramagnetic centers is also available from the Xe line shapes. At low Xe occupancy, the hyperfine contribution to the span is proportional to the *concentration* of paramagnetic centers, thus the observed overall span, $(\delta_{\|}-\delta_{\perp})$, also increases with concentration of paramagnets.

In addition to these signatures, we have made several observations in our simulations, illustrated in the figures, which would indicate the relative sensitivity of the various aspects of the Xe line shapes (the span, the $\delta_{\perp}$ component, the $\delta_{\|}$ component, the additional isotropic shift arising from the Fermi contact interaction) to various characteristics of the paramagnetic centers in the channel:

In the limit of nearly zero occupancy, the span increases with increasing concentration of paramagnetic centers, and it increases with decreasing temperature, for any orientation of the paramagnetic center.

The component of the tensor perpendicular to the axis of the channel, $\delta_{\perp}$, is sensitive to several structural factors: the orientation of the paramagnetic centers, the distribution of the paramagnetic centers, the average distance of the paramagnetic centers from the axis of the channel. (a) The $\delta_{\perp}$ component is larger when the axes of the paramagnetic centers are perpendicular to the channel axis, than for the parallel orientation. (b) Where the proximity of the paramagnetic centers of the neighboring channels is such as to provide effectively twice the concentration seen by Xe from a single channel (as it is in model A), the $\delta_{\perp}$ component is nearly identical to that in model E which has twice the concentration of paramagnetic centers within the same channel compared to model B. (c) The $\delta_{\perp}$ component goes toward more negative values (for the paramagnetic axis parallel to the axis of the channel) for shorter radial distance of the paramagnetic center from the center of the channel.

When the axis of the paramagnetic center is parallel to the channel axis, the component of the tensor parallel to the axis of the channel, $\delta_{\|}$, is sensitive to several structural factors: the concentration of paramagnetic centers in the channel and the average distance of the paramagnetic centers from the axis of the channel. The $\delta_{\|}$ component is negative and goes to significantly more negative values for increasing concentration of paramagnetic centers and for shorter radial distance of the paramagnetic center from the center of the channel. As temperature is decreased, these trends become more pronounced.

DISCUSSION

Some of the signature line shape characteristics we have discovered are for Xe at near-zero occupancy in the channel. This may be difficult to observe when using natural abundance thermally polarized ^{129}Xe. For those cases where the Xe line shapes in the undoped but otherwise identical diamagnetic channels can be observed, we recommend a procedure: Observe the Xe NMR spectra in a physical mixture of doped and undoped channels at equilibrium. If the crystallites are large enough that the exchange of Xe between two crystallites is slow, then both line shapes will be observed, undistorted by Xe exchange. The chemical potential of the Xe in the overhead gas and of the occluded Xe in all of the crystallites of both types will be the same at equilibrium. If the channel structure is identical (at low doping, they may well be) then the Xe occupancy in doped channels nearly equals the Xe occupancy in the undoped channels. In this case, the contributions coming from Xe–Xe interactions and Xe-diamagnetic channel atom interactions will be nearly identical in both doped and undoped channels. The relative amounts of crystallites of each type will influence the overall intensities of each shape, but not the singularities of the respective powder patterns. Subtraction of chemical shift tensor components between the two line shapes will provide the hyperfine contribution; that is

$$\delta_{\|}(\text{hyperfine}) = \delta_{\|}(\text{doped}) - \delta_{\|}(\text{undoped}),$$

$$\delta_{\perp}(\text{hyperfine}) = \delta_{\perp}(\text{doped}) - \delta_{\perp}(\text{undoped}).$$

The answers should be the same for every sample and at every Xe occupancy, if the occupancies are indeed the same for doped and undoped channels. The standard deviation obtained from a series of measurements at various occupancies will signify whether the premise of equality of contributions coming from Xe–Xe interactions and Xe-diamagnetic channel atom interactions in the doped and undoped crystals needs to be re-examined. A small difference in adsorption isotherms of doped and undoped channels will lead to a measurable uncertainty in the average values of $\delta_{\|}$ (hyperfine) and $\delta_{\perp}$ (hyperfine).

In this work we have used Ne as a convenient electronic model for a typical atom of the channel wall, which provides a much smaller response in diamagnetic channels than is typical of zeolites, $ALPO_4$ channels, or dipeptide channels. The systematic change in Xe line shapes in going to the electronic structure of more typical wall atoms in inorganic, organic, and biological materials has been described separately.[17] The use of Ne as a model does not alter the

discussions and conclusions in this work because in each model channel we have separately calculated the line shapes for the diamagnetic channel that has all the same shielding responses, including those coming from the O atoms, except that the hyperfine contributions have been zeroed out.

In this work we have used O_2 as a convenient model paramagnetic center, using the quantum mechanically calculated $Xe@O_2$ hyperfine response as the sole source of spin density. In a real physical system, the embedded dopant could spread the spin density through overlap, exchange, and electron correlation, to the nearby atoms as well. At high dopant concentrations the hyperfine effects will therefore become nonlinear with dopant concentration as the spin density becomes delocalized throughout the channel. We have not included this quantum mechanical delocalization of electron spin density in our modeling. Thus, our results exhibit the proximity of the paramagnetic centers to Xe more clearly. Where spin delocalization to other channel atoms is significant, even those paramagnetic centers several atoms removed from the channel walls can influence the Xe line shapes directly through the spin density delocalized onto the channel wall atoms.

Furthermore, for Xe at a paramagnetic center of symmetry higher or lower than O_2, the mathematical surface describing the hyperfine tensor can have different spatial symmetry. Thus, other models for paramagnetic centers need to be considered as well. For the particular example of the $[Cr(en)_3]^{3+}$ paramagnetic centers,[12] the magnitude and the spatial symmetry of the spin density on the ethylenediamine ligand determines the Xe hyperfine response, since the electrons of the Xe atom in the channel can overlap significantly with only the C and H atoms of this ligand. A quantum mechanical calculation of Xe approaching the C and H atoms of $[Cr(en)_3]^{3+}$ from directions that are permitted for a Xe atom in the channel will provide the response tensor surface that can be used in Monte Carlo simulations of the Xe line shapes in the dehydrated $[Cr(en)_3]^{3+}Cl_3$ crystal. As a first approximation, a smaller radical which has very nearly the same C and H hyperfine tensors may suffice as a simple model, in the same way that the quantum mechanically calculated diamagnetic shielding surface of $Xe@CH_4$ was used to provide Xe–C and Xe–H shielding response tensor surfaces which permitted a first order estimate of the Xe line shapes for Xe in the channels of dipeptide molecular crystals to be calculated.[16]

CONCLUSIONS

Using model channels and model paramagnetic centers for which the Xe shielding and hyperfine tensor response functions have been quantum-mechanically calculated as a function of configuration, we have established that NMR line shapes of Xe in nanochannels can easily distinguish among various characteristics of paramagnetic centers in porous solids, such as the concentration of paramagnetic centers in the solid, the orientation of the axis of the paramagnetic center relative to the axis of the channel, the average distance of the paramagnetic centers from the channel axis, and the distribution of paramagnetic centers in the channel and throughout the solid. Xe line shapes can vary in profound ways when these characteristics are changed, and when the temperature is changed. Furthermore, we have found some rules of thumb about the tensor components which serve as line shape signatures; that is, they permit us to infer *a priori*, something definite about the presence and the orientation of paramagnetic centers in our porous solid, upon observing the Xe line shapes at near zero occupancy, or as a function of temperature, or as a function of occupancy. We have not addressed paramagnetic centers of different symmetry than axial, and we have not considered distributions of paramagnetic centers that are not symmetrically substitutional in the channel.

ACKNOWLEDGMENTS

This work has been supported in part by the National Science Foundation (Grant No. CHE-9979259). D.N.S. thanks the Alberta Ingenuity Fund and the I. W. Killam Fund for postdoctoral fellowships. L.V. is grateful for the Herbert E. Paaren Scholarship during the course of this work at UIC.

[1] M. E. Davis, Nature (London) **417**, 813 (2002).
[2] P. J. Langley and J. Hulliger, Chem. Soc. Rev. **28**, 279 (1999).
[3] D. T. Bong, T. D. Clark, J. R. Granja, and M. R. Ghadiri, Angew. Chem., Int. Ed. **40**, 988 (2001).
[4] R. Tenne and C. N. R. Rao, Philos. Trans. R. Soc. London, Ser. A **362**, 2099 (2004).
[5] D. Maspoch, D. Ruiz-Molina, K. Wurst, C. Rovira, and J. Veciana, Chem. Commun. (Cambridge) **2004**, 1164.
[6] D. Maspoch, D. Ruiz-Molina, and J. Veciana, J. Mater. Chem. **14**, 2713 (2004).
[7] S. Horike, R. Matsuda, R. Kitaura, S. Kitagawa, T. Iijima, K. Endo, Y. Kubota, and M. Takata, Chem. Commun. (Cambridge) **2004**, 2152.
[8] Y. Li, G. H. Li, G. W. Meng, L. D. Zhang, and F. Phillipp, J. Phys.: Condens. Matter **13**, 2691 (2001).
[9] J. L. Bonardet, J. Fraissard, A. Gedeon, and M. A. Springuel-Huet, Catal. Rev. - Sci. Eng. **41**, 115 (1999).
[10] C. I. Ratcliffe, *Annual Reports on NMR Spectroscopy*, edited by G. A. Webb (Academic, London, 1998), Vol. 36, pp. 123–221.
[11] B. M. Goodson, J. Magn. Reson. **155**, 157 (2002).
[12] R. E. Wasylishen, presented at the XEMAT2003 International Symposium on Xenon NMR of Materials, La Colle-sur-Loup, May 2003, pp. 29–31; D. N. Sears and R. E. Wasylishen, presented at Pacifichem 2005, Honolulu, HI, December 15–20, 2005.
[13] R. Grosse, B. Burmeister, B. Boddenberg, A. Gedeon, and J. Fraissard, J. Phys. Chem. **95**, 2443 (1991).
[14] C. J. Jameson, J. Chem. Phys. **116**, 8912 (2002).
[15] C. J. Jameson, J. Am. Chem. Soc. **126**, 10450–10456 (2004).
[16] I. Moudrakovski, D. V. Soldatov, J. A. Ripmeester, D. N. Sears, and C. J. Jameson, Proc. Natl. Acad. Sci. U.S.A. **101**, 17924 (2004).
[17] D. N. Sears and C. J. Jameson (unpublished).
[18] L. Vukovic, C. J. Jameson, and D. N. Sears, Mol. Phys. **104**, 1217 (2006).
[19] A. E. Hansen and T. D. Bouman, J. Chem. Phys. **91**, 3552 (1989).
[20] C. J. Jameson, D. N. Sears, and A. C. de Dios, J. Chem. Phys. **118**, 2575 (2003).
[21] See EPAPS Document No. E-JCPSA6-125-703634. This document can be reached via a direct link in the online article's HTML reference section or via the EPAPS homepage (http://www.aip.org/pubservs/epaps.html).
[22] R. J. Kurland and B. R. McGarvey, J. Mater. Res. **2**, 286 (1970).
[23] J. P. Jesson, In *NMR of Paramagnetic Molecules, Principles and Applications*, edited by G. N. La Mar, W. D. Horrocks, Jr., and R. H. Holm (Academic, New York, 1973), pp. 1–52.
[24] V. V. Simonyan, J. K. Johnson, A. Kuznetsova, and J. T. Yates, Jr., J. Chem. Phys. **114**, 4180 (2001).

[25] R. L. Rowley *Statistical Mechanics for Thermophysical Property Calculations* (Prentice-Hall, Englewood Cliffs, NJ, 1994).
[26] W. E. Carlos and M. W. Cole, Surf. Sci. **91**, 339 (1980).
[27] V. Aquilanti, D. Ascenzi, D. Cappelletti, M. de Castro, and F. Pirani, J. Chem. Phys. **109**, 3898 (1998).
[28] R. A. Aziz and M. J. Slaman, Mol. Phys. **57**, 825 (1986).
[29] J. Mason, Solid State Nucl. Magn. Reson. **2**, 285, (1993).
[30] N. Bloombergen and T. J. Rowland, Phys. Rev. **97**, 1679 (1955).
[31] C. J. Jameson and A. C. de Dios, J. Chem. Phys. **116**, 3805 (2002).
[32] J. A. Ripmeester and C. I. Ratcliffe, J. Phys. Chem. **99**, 619 (1995).
[33] I. L. Moudrakovski, C. I. Ratcliffe, and J. A. Ripmeester, Appl. Magn. Reson. **10**, 559 (1996).